Maximum Torque per Ampere Control Strategy for Low-Saliency Ratio IPMSMs

M. Caruso, A. O. Di Tommaso, R. Miceli, *Member IEEE*, C. Nevoloso, C. Spataro, *Member IEEE* and M. Trapanese, *Member IEEE*

*Department of Energy, Information Engineering and Mathematical Models, University of Palermo, Palermo, Italy

(massimo.caruso16@unipa.it, antoninooscar.ditommaso@unipa.it, rosario.miceli@unipa.it, claudio.nevoloso@unipa.it, ciro.spataro@unipa.it, marco.trapanese@unipa.it)

Corresponding Author: Massimo Caruso, Department of Energy, Information Engineering and Mathematical Models, University of Palermo, Palermo, Italy, Viale delle Scienze, Ed.9, 90128 Palermo, Italy. massimo.caruso16@unipa.it

Received: 24.01.2019 Accepted:10.03.2019

Abstract- This paper deals with electrical drives employing low-saliency ratio interior permanent magnet synchronous motors. In particular, in order to help the designers choosing the best control algorithm, the performances of the Maximum Torque Per Ampere Control (MTPA) and the Field Orientation Control (FOC) are here both theoretically and experimentally assessed and compared, by using, as performance indicators, the torque-current ratio and the power losses. The tests are carried out on a low-power motor for various speeds and loads by implementing the two control strategies in a dSPACE® rapid prototyping system. The results show that the Maximum Torque Per Ampere algorithm has some appreciable advantages mainly for high load conditions of operation.

Keywords IPMSM, MTPA control strategy, FOC algorithm, low saliency ratio machines.

1. Introduction

The permanent magnet synchronous machine is the most utilized motor for high-efficiency electric drives, when a variable speed and/or load are required [1-3]. Moreover, thanks to the continuous improvement of the control strategies used to obtain the target speed and torque by regulating the input voltages and currents, the applications of this motor typology are constantly growing. The IPMSMs (Interior Permanent Magnet Synchronous Motors) are widely employed because of their very good performances in terms of power losses, power factor and power density [4-10]. Indeed, the magnetic anisotropy of these motors generates an additional torque component that can be advantageously used for several applications [11-12]. The higher is the magnetic saliency, the higher will be this torque component. However, an interesting study [13], made for IPMSM with distributed windings, demonstrates that the high manufacturing costs related to the production of motors with high saliency ratio are justified only for applications where high performances are required. In [14], the inductance and saliency ratio of IPMSM with fractional-slot concentrated-windings with different slot and pole combinations are investigated. This paper demonstrates that the over mentioned IPMSM configurations have a poor saliency ratio, but a low manufacturing cost. For these reasons, in the fields of application where the economic requirement is extremely relevant, the use of IPMSM with a low-saliency ratio is essential. For example, in the production of light and hybrid electric vehicles where high performance is not required, the optimal choice is the usage of low-saliency ratio motors. In particular, for the mass production, where reducing the manufacturing costs is one of the most important objective, the small increase of the motor performances does not justify the great cost increase. These observations can be also applied to other fields of application.

Another way to increase the performances of an IPMSM drive and to maximize its efficiency is the implementation of innovative control algorithms. In the automotive, automation and robotic industries, a widespread control algorithm is the Field Oriented Control (FOC) algorithm, which allows the separated control of the generated torque and the magnetic flux of the machine [15-18]. This vector control strategy has a simple and flexible structure and it is currently well established. Another control strategy, largely discussed in literature, is the Maximum Torque Per Ampere (MTPA) algorithm that maximizes the electromagnetic torque for a

stated value of the stator current. The work in [19] presents a flux weakening control algorithm with maximum torque per ampere (MTPA) control for high-speed operations of an IPMSM drive. Ahmed *et al* [20] proposed a MTPA control scheme, based on power DC-link power measurement that does not require the feedback of the armature currents. This control algorithm employs a search control algorithm, which makes it robust towards parametric variations. In [21] a MTPA control method based on V/f algorithm control is discussed. The used approach employs an open-loop speed control and monitors the reactive power to regulate the current displacement. The MTPA system is almost exclusively implemented to control the IPMSM with high values of saliency ratio (> 2), since for machines with low values of saliency ratio, it seems not to produce substantial results [22-23]. Another reason that limited the use of the MTPA system in automotive and industrial applications is the complexity of this control system when compared with a traditional Field Orientation Control (FOC).

However, by considering that the adoption of a MTPA control does not require any upgrade of the electrical drive hardware, but only a reprogramming of its software part, even a small increase of the drive efficiency could justify the increased complexity of the system. Therefore, with the aim to assess if and how much a MTPA control can rise the performances of a low saliency ratio IPMSM, in a previous work [24] the Authors presented the results of a simulation analysis performed to compare the FOC and the MTPA control in terms of torque-current ratio and power losses. In order to validate these results, this paper presents the previously mentioned comparison that has been also experimentally validated.

The tests are performed on a 750 W IPMSM with low-saliency ratio, implementing both algorithms by using a rapid prototyping board. Then, the comparison is performed for several values of load and speed.

After the description of the two control algorithms and the methodology of implementation (Section II), Section III deals with the test bench set-up used for the tests. Section IV reports the results of the experimental comparison, providing also critical discussions.

2. Implementation of the proposed Approach

2.1. Control Strategies

The implementation of both FOC and MTPA strategies requires a mathematical model of the machine. Usually, in order to make independent the motor parameters from the rotor position, the model is expressed in a *d-q* coordinate system, applying the Park transformation. A deep description of the circuital and mathematical model can be found in [25]. The equations concerning both the electrical balance and the electromagnetic torque are hereinafter reported:

$$V_d = RI_d + L_d \frac{dI_d}{dt} - \omega_e L_q I_q \quad (1)$$

$$V_q = RI_q + L_q \frac{dI_q}{dt} + \omega_e \lambda_{PM} + \omega_e L_d I_d \quad (2)$$

$$T_e = \frac{3}{2} p\left[\lambda_{PM} I_q - \left(L_d - L_q\right) I_d I_q\right] \quad (3)$$

For the setting of the dynamic model, the following quantities are used:

- V_d and V_q are the components of the stator phase voltages along the direct and quadrature axes, respectively;
- I_d and I_q are the components of the stator phase currents along are the direct and quadrature axes, respectively;
- p corresponds to the number of pole pairs;
- θ_m is the mechanical angular position of the rotor;
- ω_m is the mechanical angular speed of the rotor;
- ω_e is the electrical angular speed;
- λ_{PM} is the stator flux linkage due to the permanent magnets;
- R is the average value of the three-phase stator winding resistance;
- L_d and L_q are the inductances along the direct and quadrature axes, respectively;
- T_e represents the electromagnetic torque;
- T_m corresponds to the load torque;
- F is the coefficient of viscous friction;
- J is the moment of inertia.

The tested electrical drive employs a six poles, three-phase, IPMSM (Fig. 1). The motor is equipped by samarium-cobalt permanent magnets, which are radially mounted on the rotor and circumferentially magnetized. The double-layer stator windings are placed in 27 slots (Fig. 2).

The parameters adopted for the mathematical model have been determined from a series of measurements and tests performed in order to accurately characterize the motor [22].

Table 1 reports the values of the motor parameters, whereas Table 2 reports the IPMSM geometrical data. Fig. 3 and 4 show the block schemes of the MTPA-based system and of FOC-based system, respectively.

In the MTPA-based system, the speed error, namely the difference between the reference speed ω^* and the actual rotor speed ω, which has been measured through a resolver, is computed by the block named "Speed controller". The "MTPA" block calculates the instantaneous values of i_d^* and i_q^*, which maximizes the electromagnetic torque. The calculated currents are compared in the "Current controller" block with the actual input currents and, as a result of this

comparison, the reference values Park components for the supply voltage v_d^* and v_q^* are obtained. Then, the v_d^* and v_q^* values are re-transformed in a three-phase reference system, by applying the inverse Park transformation and, finally, applied to the motor with a PWM technique. The transformation of the voltage and current quantities from a three-phase reference system to a *d-q* rotating reference system is obtained through the following Park direct and inverse transformation matrices:

$$T_{dir} = \frac{2}{3}\begin{bmatrix} \cos\vartheta & \cos\left(\theta-\frac{2}{3}\pi\right) & \cos\left(\theta-\frac{4}{3}\pi\right) \\ -\sin\theta & -\sin\left(\theta-\frac{2}{3}\pi\right) & -\sin\left(\theta-\frac{4}{3}\pi\right) \\ \frac{1}{2} & \frac{1}{2} & \frac{1}{2} \end{bmatrix} \quad (4)$$

$$T_{inv} = \begin{bmatrix} \cos\vartheta & -\sin\theta & 1 \\ \cos\left(\theta-\frac{2}{3}\pi\right) & -\sin\left(\theta-\frac{2}{3}\pi\right) & 1 \\ \cos\left(\theta-\frac{4}{3}\pi\right) & -\sin\left(\theta-\frac{4}{3}\pi\right) & 1 \end{bmatrix} \quad (5)$$

where θ is the angle between the direct axis and the magnetic axis of the reference phase winding. The FOC system has the same hardware structure to the MTPA system and it is able to set the direct component of the stator current, allowing the variation of the magnetization level of the machine, reinforcing ($i_d > 0$) or counteracting ($i_d < 0$) the magnetic field generated by the permanent magnets. The main difference between the two control algorithms concerns the determination of the *d-q* reference currents to satisfy the load condition of the IPMSM. For the comparison proposed in this work, the FOC operates by setting $i_d = 0$. The instantaneous value of i_q^* is obtained from eq. (1).

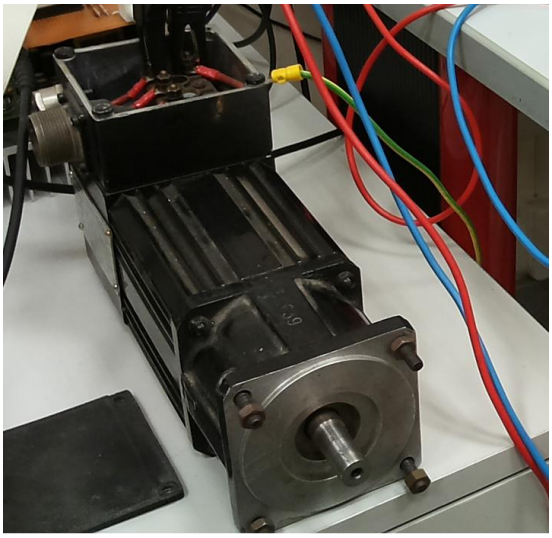

Fig. 1. The motor under test.

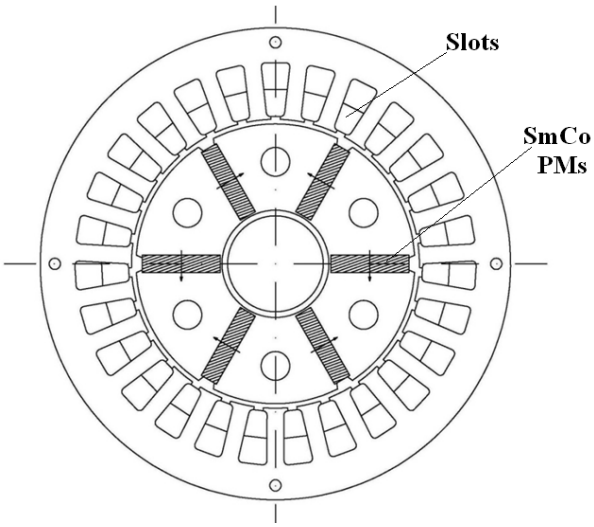

Fig. 2. The IPMSM cross-section.

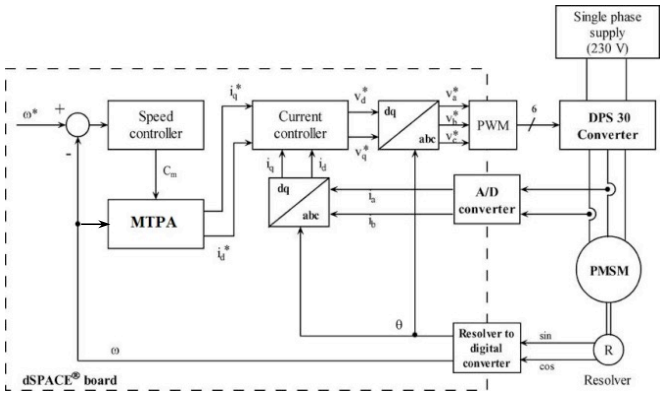

Fig. 3. Block scheme of the MTPA control strategy.

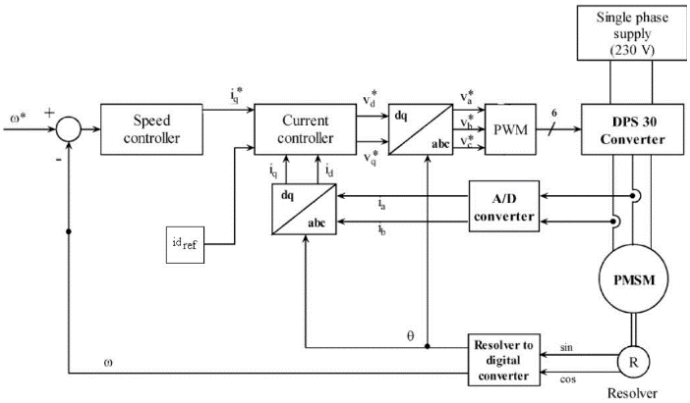

Fig. 4. Block scheme of the FOC control strategy (i_d=0).

Table 1. IPMSM Rated values and computed parameters

Rated voltage	132 V
Rated current	3.6 A
Rated speed	4000 rpm
Rated torque	1.8 N·m
Nr. of pole pairs	3
Stator resistance (average value)	2.21 Ω
Inductance along the direct-axis	9.77 mH
Inductance along the quadrature axis	14.94 mH
stator flux linkage due to PMs	0.084 Wb
Coefficient of viscous friction	0.001 N·m·s
Inertia moment of inertia	0.001 kg·m^2

Table 2. IPMSM geometrical data

Outer stator diameter	81 mm
Inner stator diameter	49.6 mm
Outer rotor diameter	48 mm
Inner rotor diameter	18.46 mm
Axial rotor length	59 mm
PM width	13.45 mm
PM thickness	3 mm
Air gap	0.8 mm
Slot depth	9.2 mm

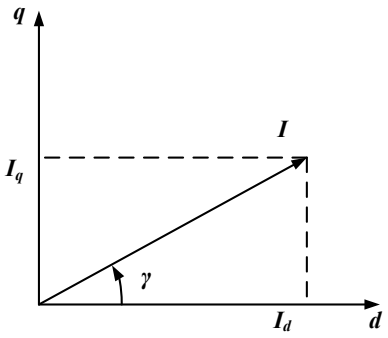

Fig. 5. Diagram of the currents.

2.2. *MTPA Algorithm Equations*

The goal of this section is the description of the mathematical approach employed in order to achieve the equations of the MTPA algorithm. The expression of the electromagnetic torque (eq. (3)), obtained by rearranging the equations referred to the current components (see Fig. 5), is given by:

$$T_e = \frac{3}{2}p\left[\lambda_{PM} I \sin\gamma + \left(L_d - L_q\right) I^2 \sin\gamma \cos\gamma\right] \tag{6}$$

By taking the derivative as a function of the angle γ and by setting it equal to zero, the stator current value that maximizes the electromagnetic torque is obtained:

$$\lambda_{PM} I \cos\gamma + \left(L_d - L_q\right) I^2 [(\cos\gamma)^2 - (\sin\gamma)^2] = 0 \tag{7}$$

Eq. (7) can be rewritten as a function of both the I_d and I_q components, obtaining the following formula:

$$I_d^2 + \frac{\lambda_{PM}}{\left(L_d - L_q\right)} I_d - I_q^2 = 0 \tag{8}$$

In order to obtain the reference values of *d-q* axes currents, by combining eq. (3) and eq. (8), the following equation is obtained, which are expressed only as a function of I_q:

$$I_{qref}^4 + \frac{T_e \lambda_{PM}}{\frac{3}{2}p\left(L_d - L_q\right)^2} I_{qref} - \frac{{T_e}^2}{\left[\frac{3}{2}p\left(L_d - L_q\right)\right]^2} = 0 \tag{9}$$

From this equation, it is possible to evaluate the value of I_{qref} that satisfies the required torque from the machine in stationary conditions. The calculation of the solutions can be easily obtained by means of any symbolic computation program, such as Matlab®, by also adopting the values of the motor parameters described in Tables 1-2.

The reference current value I_{dref} can be simply determined by replacing the determined solution in eq. (8):

$$I_{dref} = -\frac{\lambda_{PM}}{2\left(L_d - L_q\right)} - \sqrt{\left(\frac{\lambda_{PM}}{2\left(L_d - L_q\right)}\right)^2 + I_{qref}^2} \tag{10}$$

The locus of points that maximizes the torque/current ratio in a I_d-I_q plane is represented in Fig. 6, together with the trend of eq.(3), for fixed values of electromagnetic torque. In

particular, eq. (3) describes an equilateral hyperbola, whose asymptotes are given by:

$$I_d = -\frac{\lambda_{PM}}{(L_d - L_q)} \tag{11}$$

$$I_q = 0 \tag{12}$$

In this way, the intersection between the locus of points that maximizes the torque/current ratio and the torque curve allows the determination of the optimum values of the *d-q* axis currents. Obviously, it is necessary to taking into account the voltage and current limits of the electrical drive, imposing that:

$$\sqrt{I_d^2 + I_q^2} \leq I_x \tag{13}$$

$$\sqrt{V_d^2 + V_q^2} \leq V_x \tag{14}$$

being I_x and V_x the maximum allowed current and the maximum allowed voltage, respectively, which depend on the characteristics of both converter and motor. These maximum allowed values have been chosen by considering the features of the motor, since the rated voltage and rated current of the used inverter are higher than those of the motor (see Table 3). More in detail, eq. (13), which is related to the current limit, represents a circumference with the center at the coordinates *(0;0)* and a radius equal to I_x in the I_d-I_q plane. Instead, by substituting eq. (1-2) in eq. (14), it is possible to obtain the following equation in a steady-state condition:

$$p\omega_m\sqrt{(\lambda_{PM} + L_d I_d)^2 + \left(L_q I_q\right)^2} \leq V_x \tag{15}$$

Eq. (15) represents the equation of an ellipse with the center at the coordinates $(-\lambda_{PM}/L_d;0)$, with a radius parallel to the I_q-axis equal to $(V_x/p\omega_m L_q)$ and a radius parallel to the I_d-axis equal to $(V_x/p\omega_m L_d)$.

The voltage limit, which is represented by the ellipse, reduces its size as the motor speed increases. Therefore, it is not needed to take into account the voltage limit for all the mechanical speed values (Fig. 7). The speed limit, corresponding to the value for which the voltage limit cannot be no more ignored, is determined by the intersection of the voltage limit, current limit and MTPA curves (see points A and B of Fig. 8). In particular, the speed limit is given by the following relationship:

$$\omega_{ml} = \frac{V_x}{p\sqrt{\left((\lambda_{PM} + L_d I_d)^2 + \left(L_q I_q\right)^2\right)}} \tag{16}$$

where I_{dl} and I_{ql} are the coordinates of points A and B in the I_d-I_q plane. Fig. 9 shows the curve referred to the MTPA, the curve of the current limit, the curves of constant torque and the limit voltage curves for different mechanical speed values.

Finally, the MTPA algorithm is structured by the following steps:

- From the reference value of the torque, which is obtained from the speed error, the MTPA algorithm calculates the optimal values of the *d-q* reference currents I_{dref} and I_{qref};
- The mechanical speed of the machine is compared with the mechanical speed limit (see eq. (8)) and, from this comparison, the limit values of the *d-q* axes currents are evaluated either from the current limit or from the voltage limit equations;
- The previous steps allow to fix the maximum allowed reference current values, I_{dref} and I_{qref}.

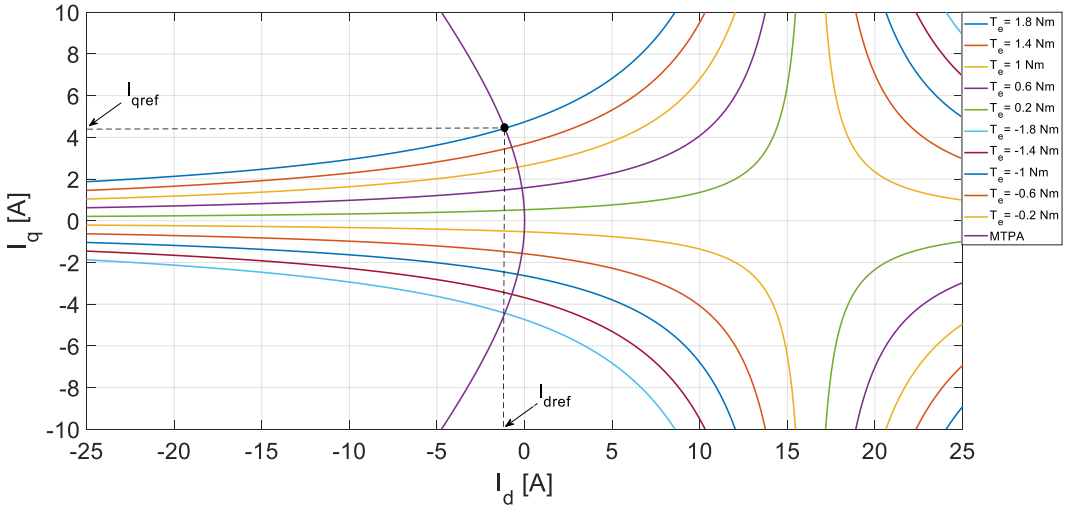

Fig. 6. Constant torque and maximum torque/current ratio operating curves.

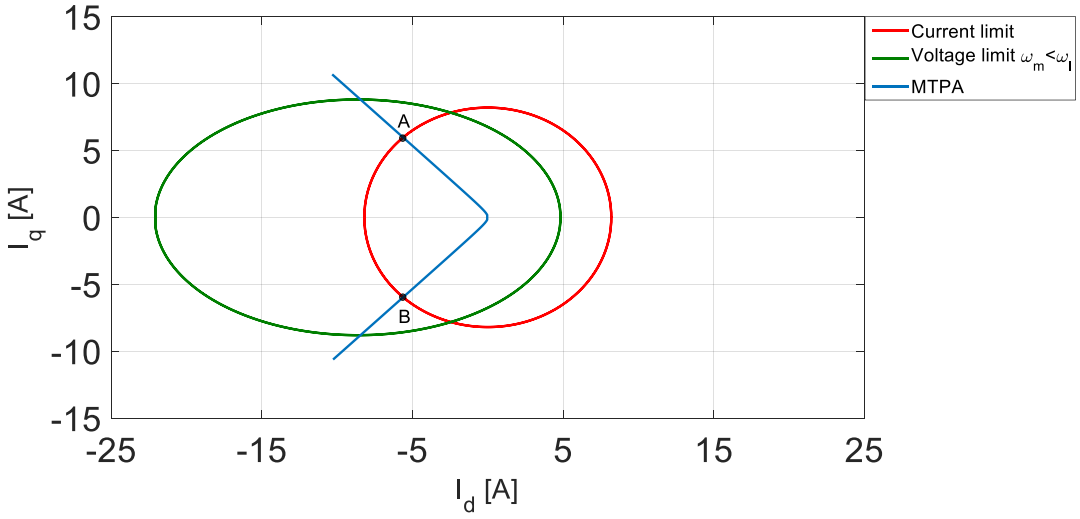

Fig. 7 Voltage, current limits and maximum torque/current ratio operating curves for $\omega_m<\omega_{ml}$.

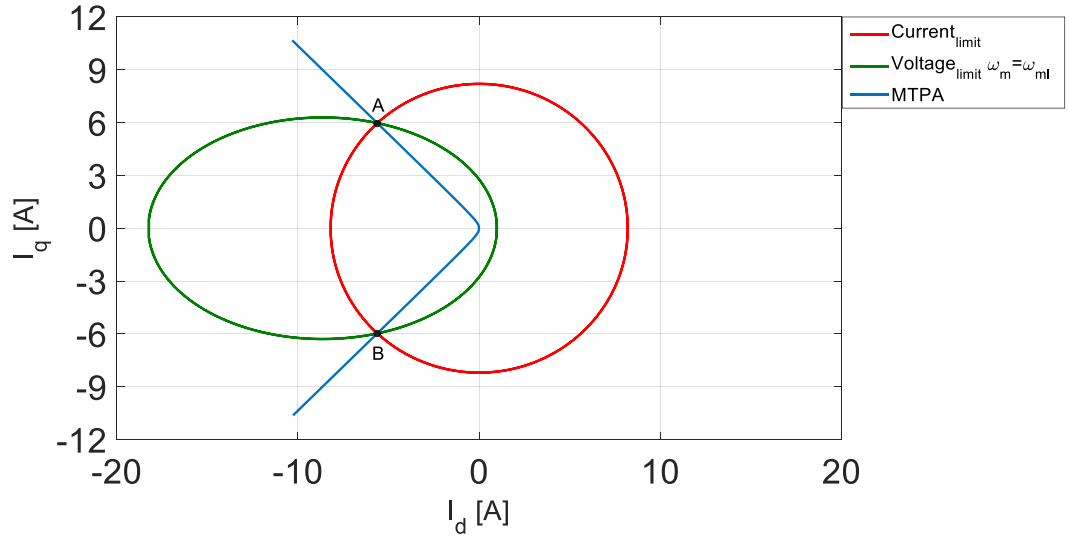

Fig. 8. Voltage, current limits and maximum torque/current ratio operating curves for $\omega_m=\omega_{ml}$.

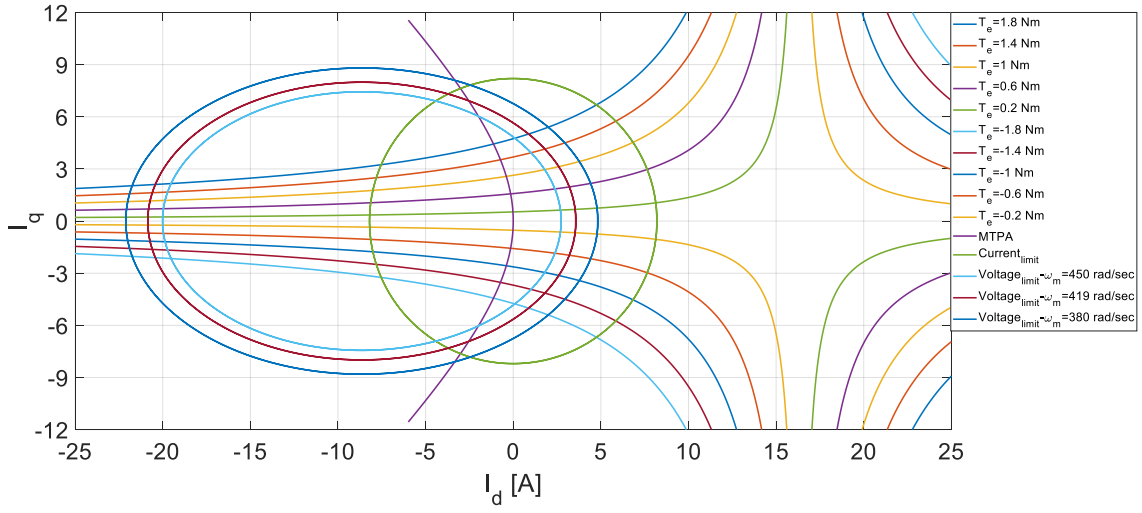

Fig. 9. Current limit, maximum torque/current ratio operating curves and voltage limit operating curves for different values of mechanical speed.

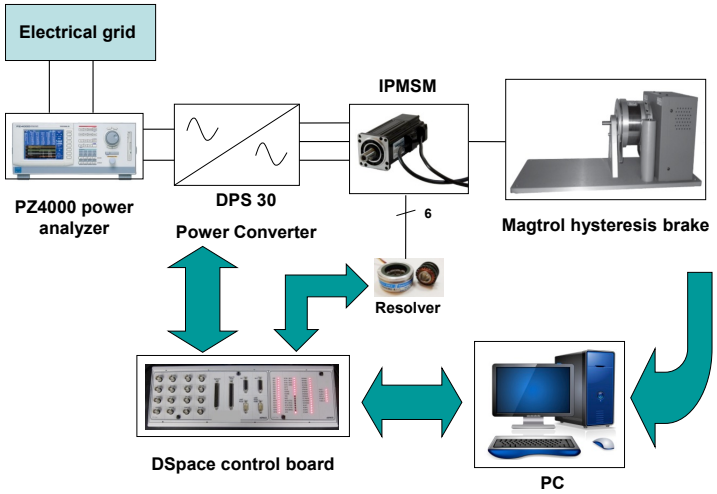

Fig. 10. Schematic representation of the test bench.

3. Test Bench Equipment

With the aim of validating the proposed approach and the simulation results, various tests and measurements were carried out. Fig. 10 shows a graphic representation of the used test bench.

The motor under test is driven by an Automotion Inc. DPS 30-A inverter, which is controlled by a dSPACE® prototyping control board. The inverter is equipped with two LEM current sensors, which are used to acquire the instantaneous values of the three-phase supply currents of the IPMSM. Table 3 reports the main data of the DPS 30 A inverter.

Table 3. Main data of the DPS 30 A inverter

Model	DSP 30 A
Input voltage [V]	230
Peak output current [A]	30
Maximum output power [kVA]	6.5
DC-link voltage [V]	310
Switching frequency [kHz]	5-20
Current sensors (F. W. Bell)	CLN-25

The motor load is generated by an hysteresis brake (MAGTROL HD-715), which is controlled by a high-speed programmable dynamometer (MAGTROL DSP6001), allowing the variations of the load conditions.

The rotational speed of the motor is measured by means of an ARTUS 26SM19U452 COIF/OO, connected to the motor shaft.

Currents, voltages and input active power are measured by means of a Yokogawa PZ 4000 three-phase power analyzer.

The voltage and current signals are sampled by setting the analyzer frequency rate at 1 MS/s. In the frequency range of the acquired signals, the PZ 4000 guarantees an expanded measurement uncertainty (assessed using a coverage factor k = 3) equal to:

- (0.2 % of reading + 0.5 V) for the voltage measurements;
- (0.2 % of reading + 0.02 A) for the current measurements;
- (0.5 % of reading + 1 W) for the voltage measurements.

4. Experimental results

With the purpose of comparing the torque-current ratio of the proposed control strategies, various measurements were performed on the motor under test for several steady-state working conditions. In particular, the rotor speed was changed in the range 500 ÷ 4000 rpm, with steps of 500 rpm. For each of these eight speed values, six values of load torque were applied to the motor shaft, starting from 0% to a 100% of its rated load with steps of 20%. For each of the 40 working conditions, both the MTPA and the FOC control algorithm were employed. The graphs referred to the torque-current ratio as a function of the rotor speed, parameterized for various loads, are shown in Fig. 11 and Fig. 12. The

analysis of the plots indicates that, for the low values of load, the torque-current ratio of the two approaches are practically very close, whereas, for high values of load, the MTPA strategy achieves a better performance than the FOC. To compare easily the two torque-current ratio trends, it is worthwhile to define the following quantity:

$$T_e/I_{rms}\,\% = \frac{T_e/I_{rms_{MTPA}} - T_e/I_{rms_{FOC}}}{T_e/I_{rms_{FOC}}}\,100 \qquad (17)$$

where T_e/I_{rmsFOC} and $T_e/I_{rmsMTPA}$ are the torque-current ratio obtained with the FOC and the MTPA strategies, respectively.

Table 4 reports the values of the $T_e/I_{rms}\%$ for each stationary working condition. Again, it is possible to observe that the MTPA ensures a higher torque-current ratio mainly at high loads, especially at both 80% and 100% of rated torque. Obviously, a better torque-current ratio entails an increase of the motor efficiency. Therefore, an experimental investigation on the IPMSM power losses for each load and speed condition has been carried out by applying the proposed control techniques. The power losses have been evaluated as a difference between the input electrical power, measured with the three-phase power analyzer, and the mechanical power, measured with the dynamometer. For instance and for various speed values, the power losses are reported as a function of the load in Figs. 12 and 13. For each working conditions and for both algorithms, the trends of the motor efficiency are practically identical. However, for all the considered cases, the power losses are lower when the electrical drive is controlled by the MTPA algorithm. Even if for low load values the amplitude of the difference between the power losses of the two control algorithms is not very appreciable, this difference increases when the value of the applied load raises. The same conclusions can be drawn from the plots of Fig. 14, which reports the power losses as a function of the torque for various speed values. As previously discussed, it possible to notice that the FOC approach entails a higher power consumption respect to the MTPA strategy, mainly for the higher speed values.

The obtained results show that the MTPA control strategy is suitable to the FOC approach even for low-saliency ratio motors, mainly for high values of load and speed. Instead, at low loads, the performances of the two algorithms are almost comparable.

5. Conclusions

This paper has presented an experimental investigation and comparison on the performances provided by the MTPA and the FOC techniques. The experimental analisys was carried out on a low saliecncy ratio IPMSM. The torque-current ratio and the power losses have been taken into consideration as terms of comparison for the performance evaluation between the two control techniques. The results have shown that the MTPA technique provides higher torque-current ratio with respect to the FOC technique. Moreover, the difference between the torque-current ratios given by the two control algorithms is higher for increased values of both the applied load and mechanical speed. This result leads to a better efficiency of the machine when it is controlled with the MTPA algorithm. At low speeds and small applied loads, the performances of the two algorithms are comparable.

This experimental study can be useful in order to adequately choose the best control algorithm for an IPMSM in dependance of the related application, especially for low-saliency ratio motors.

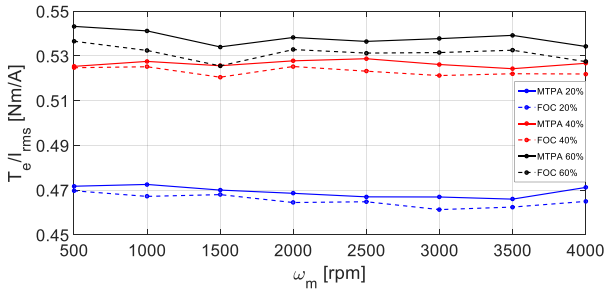

Fig. 11 Torque-current ratio vs speed at low-load conditions.

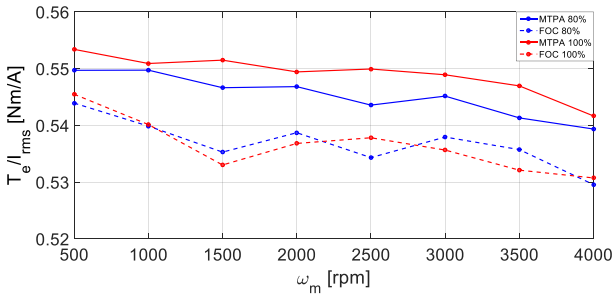

Fig. 12 Torque-current ratio vs speed at high-load conditions.

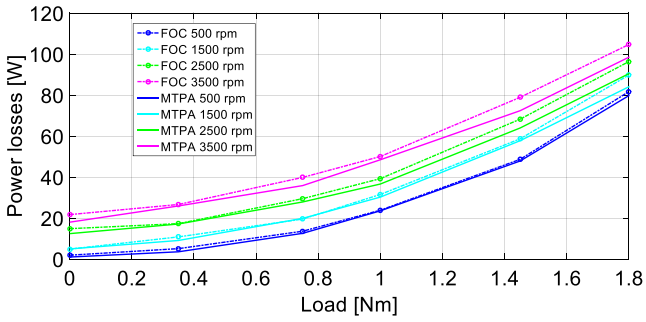

Fig. 13 Power losses vs load for various speed conditions.

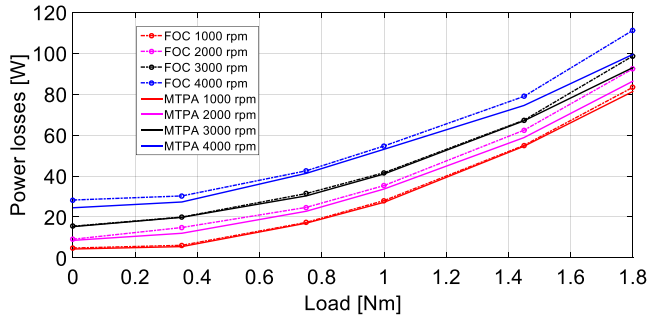

Fig. 14. Power losses vs load for various speed conditions.

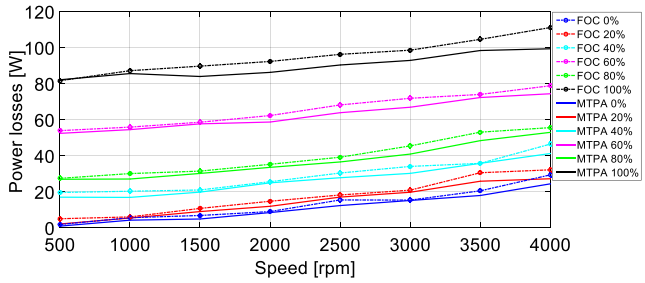

Fig. 15 Power losses vs mechanical speed for various load conditions.

Table 4. Percentage torque-current ratio difference

ΔT$_e$/Irms%	***Load torque***				
Speed [rpm]	20%	40%	60%	80%	100%
500	+0.43	+0.13	+1.24	+1.06	+1.45
1000	+1.14	+0.51	+1.64	+1.82	+1.99
1500	+0.43	+1.09	+1.61	+2.12	+3.46
2000	+0.89	+0.55	+1.01	+1.51	+2.35
2500	+0.47	+1.19	+0.98	+1.73	+2.25
3000	+1.22	+1.07	+1.17	+1.34	+2.48
3500	+0.77	+0.49	+1.24	+1.04	+2.8
4000	+1.34	+1.02	+1.28	+1.85	+2.06

Acknowledgements

This work was financially supported by MIUR - Ministero dell'Istruzione, dell'Università e della Ricerca (Italian Ministry of Education, University and Research) and by SDESLab (Sustainable Development and Energy Saving Laboratory) of the University of Palermo. The Authors would like to thank Dr. Michele Lombardo.

References

[1] H. Lin, H. Guo and H. Qian, "Design of High-Performance Permanent Magnet Synchronous Motor for Electric Aircraft Propulsion," *2018 21st International Conference on Electrical Machines and Systems (ICEMS)*, Jeju, 2018, pp. 174-179.

[2] G. Pellegrino, A. Vagati, P. Guglielmi and B. Boazzo, "Performance Comparison Between Surface-Mounted and Interior PM Motor Drives for Electric Vehicle Application," in *IEEE Transactions on Industrial Electronics*, vol. 59, no. 2, pp. 803-811, Feb. 2012.

[3] J. J. H. Paulides, L. Encica, T. F. Beernaert, H. H. F. van der Velden, A. G. P. Parfant and E. A. Lomonova, "Ultra-light-weight high torque density brushless PM machine design: Considering driving-cycle of a four-wheel drive race car," *2015 Tenth International Conference on Ecological Vehicles and Renewable Energies (EVER)*, Monte Carlo, 2015, pp. 1-7.

[4] C. Cavallaro, A. O. Di Tommaso, R. Miceli, A. Raciti, G. R. Galluzzo and M. Trapanese, Efficiency Enhancement of Permanent-Magnet Synchronous Motor Drives by Online Loss Minimization Approaches, in IEEE Transactions on Industrial Electronics, vol. 52, no. 4, pp. 1153-1160, Aug. 2005.

[5] A. O. Di Tommaso, R. Miceli and G. Ricco Galluzzo, "Improvement of IPMSM performance through a mixed radial-tangential rotor structure," *2010 IEEE International Symposium on Industrial Electronics*, Bari, 2010, pp. 1327-1332.

[6] M. Caruso, A. O. Di Tommaso, F. Genduso and R. Miceli, "Experimental investigation on high efficiency real-time control algorithms for IPMSMs," *2014 International Conference on Renewable Energy Research and Application (ICRERA)*, Milwaukee, WI, 2014, pp. 974-979.

[7] Caruso, M., Di Tommaso, A.O., Miceli, R., Nevoloso, C., Spataro, C. & Viola, F. 2017, "Comparison of three control drive systems for interior permanent magnet synchronous motors", *22nd IMEKO TC4 International Symposium and 20th International Workshop on ADC Modelling and Testing 2017: Supporting World Development Through Electrical and Electronic Measurements*, pp. 492.

[8] B. Gallert, G. Choi, K. Lee, X. Jing and Y. Son, "Maximum efficiency control strategy of PM traction machine drives in GM hybrid and electric vehicles," *2017 IEEE Energy Conversion Congress and Exposition (ECCE)*, Cincinnati, OH, 2017, pp. 566-571.

[9] I. Boldea, L. N. Tutelea, L. Parsa and D. Dorrell, "Automotive Electric Propulsion Systems With Reduced or No Permanent Magnets: An Overview," in *IEEE Transactions on Industrial Electronics*, vol. 61, no. 10, pp. 5696-5711, Oct. 2014.

[10] T. Bariša, D. Sumina and M. Kutija, "Comparison of maximum torque per ampere and loss minimization control for the interior permanent magnet synchronous generator," *2015 International Conference on Electrical Drives and Power Electronics (EDPE)*, Tatranska Lomnica, 2015, pp. 497-502

[11] K. Roumani and B. Schmuelling, "Study on the MTPA control for a low voltage IPMSM," *2015 Tenth International Conference on Ecological Vehicles and Renewable Energies (EVER)*, Monte Carlo, 2015, pp. 1-5.

[12] M. Caruso, A. O. Di Tommaso, R. Miceli, C. Nevoloso, C. Spataro and F. Viola, "Interior permanent magnet

synchronous motors: Impact of the variability of the parameters on their efficiency," *2016 IEEE International Conference on Renewable Energy Research and Applications (ICRERA)*, Birmingham, 2016, pp. 1163-1167-.

[13] Zhang, D. M. Ionel and N. A. O. Demerdash, "Saliency Ratio and Power Factor of IPM Motors With Distributed Windings Optimally Designed for High Efficiency and Low-Cost Applications," in IEEE Transactions on Industry Applications, vol. 52, no. 6, pp. 4730-4739, Nov.-Dec. 2016.

[14] Xiaolong Zhang, Ronghai Qu, Hong Chen and Jian Luo, "Analysis of d- and q-axis inductances and saliency ratios in interior permanent magnet machines with fractional-slot concentrated- windings considering harmonic effects," *2013 International Conference on Electrical Machines and Systems (ICEMS)*, Busan, 2013, pp. 1080-1085.

[15] E. Yesilbag and L. T. Ergene, "Field oriented control of permanent magnet synchronous motors used in washers," *2014 16th International Power Electronics and Motion Control Conference and Exposition*, Antalya, 2014, pp. 1259-1264.

[16] Antony, T.M.R., Jose, J., Sakthivel, S., Jagadishan, D., Winston, S.J., Venugopal, S., “Design and development of two axis control and drive for PMSM motor of in-service inspection module for PFBR steam generator”, (2014) Procedia Engineering, 86, pp. 520-528.

[17] S. K. Dwivedi, M. Laursen and S. Hansen, "Voltage vector based control for PMSM in industry applications," 2010 IEEE International Symposium on Industrial Electronics, Bari, 2010, pp. 3845-3850.

[18] W. Peters, O. Wallscheid and J. Böcker, "Optimum efficiency control of interior permanent magnet synchronous motors in drive trains of electric and hybrid vehicles," *2015 17th European Conference on Power Electronics and Applications (EPE'15 ECCE-Europe)*, Geneva, 2015, pp. 1-10.

[19] S. Halder, S. P. Srivastava and P. Agarwal, "Flux weakening control algorithm with MTPA control of PMSM drive," *2014 IEEE 6th India International Conference on Power Electronics (IICPE)*, Kurukshetra, 2014, pp. 1-5.

[20] A.Ahmed, Y. Sozer and M. Hamdan, "Maximum Torque per Ampere Control for Buried Magnet PMSM Based on DC-Link Power Measurement," in *IEEE Transactions on Power Electronics*, vol. 32, no. 2, pp. 1299-1311, Feb. 2017.

[21] J. i. Itoh, Y. Nakajima and M. Kato, "Maximum torque per ampere control method for IPM Synchronous Motor based on V/f control," 2013 IEEE 10th International Conference on Power Electronics and Drive Systems (PEDS), Kitakyushu, 2013, pp. 1322-1327.

[22] A. Purwadi, R. Hutahaean, A. Rizqiawan, N. Heryana, N. A. Heryanto and H. Hindersah, "Comparison of maximum torque per Ampere and Constant Torque Angle control for 30kw Interior Interior Permanent Magnet Synchronous Motor," Proceedings of the Joint International Conference on Electric Vehicular Technology and Industrial, Mechanical, Electrical and Chemical Engineering (ICEVT & IMECE), Surakarta, 2015, pp. 253-257.

[23] Y. Miao, H. Ge, M. Preindl, J. Ye, B. Cheng and A. Emadi, "MTPA Fitting and Torque Estimation Technique Based on a New Flux-Linkage Model for Interior-Permanent-Magnet Synchronous Machines," in IEEE Transactions on Industry Applications, vol. 53, no. 6, pp. 5451-5460, Nov.-Dec. 2017.

[24] M. Caruso, A. O. Di Tommaso, M. Lombardo, R. Miceli, C. Nevoloso and C. Spataro, "Maximum Torque Per Ampere control algorithm for low saliency ratio interior permanent magnet synchronous motors," *2017 IEEE 6th International Conference on Renewable Energy Research and Applications (ICRERA)*, San Diego, CA, USA, 2017, pp. 1186-1191.

[25] Caruso, M., Di Tommaso, A.O., Miceli, R., Nevoloso, C., Spataro, C. & Viola, F. 2017, "Characterization of the parameters of interior permanent magnet synchronous motors for a loss model algorithm", *Measurement: Journal of the International Measurement Confederation,* vol. 106, pp. 196-202.